Materials Science and Engineering C 42 (2014) 489–499

Contents lists available at ScienceDirect

Materials Science and Engineering C

journal homepage: www.elsevier.com/locate/msec

Optimization of poly(L-lactic acid)/segmented polyurethane electrospinning process for the production of bilayered small-diameter nanofibrous tubular structures

F. Montini Ballarin [a], P.C. Caracciolo [a], E. Blotta [b], V.L. Ballarin [b], G.A. Abraham [a,*]

[a] Research Institute for Materials Science and Technology, INTEMA (UNMdP-CONICET), Av. Juan B. Justo 4302, B7608FDQ Mar del Plata, Argentina
[b] Digital Image Processing Group, School of Engineering, National University of Mar del Plata, Av. Juan B. Justo 4302, B7608FDQ Mar del Plata, Argentina

ARTICLE INFO

Article history:
Received 17 February 2014
Received in revised form 15 May 2014
Accepted 30 May 2014
Available online 5 June 2014

Keywords:
Electrospinning
Bioresorbable polyurethane
Polymer blends
Vascular grafts
Morphology

ABSTRACT

The present study is focused on the electrospinning process as a versatile technique to obtain nanofibrous tubular structures for potential applications in vascular tissue engineering. A bilayered scaffolding structure composed of poly(L-lactic acid) (PLLA)/bioresorbable segmented polyurethane (SPEU) blends for small-diameter (5 mm) vascular bypass grafts was obtained by multilayering electrospinning. Polymer blend ratios were chosen to mimic the media and adventitia layers. The influence of the different electrospinning parameters into the fiber formation, fiber morphology and fiber mean diameter for PLLA, SPEU and two PLLA/SPEU blends were studied. Flat and two-parallel plate collectors were used to analyze the effect of the electrostatic field on the PLLA nanofiber alignment in the rotating mandrel. Membrane topography resulted in random or aligned nanofibrous structures depending on the auxiliary collector setup used. Finally, composition, surface hydrophilicity, thermal properties and morphology of nanofibrous scaffolds were characterized and discussed. Since the development of tissue engineered microvascular prostheses is still a challenge, the prepared scaffolding tubular structures are promising candidates for vascular tissue engineering.

1. Introduction

Electrospinning is a powerful processing technique with great features for nanofiber manufacturing such as versatility, cost-effectiveness, potential to scale up, and ability to use a broad range of materials [1–3]. To date, many different materials have been electrospun in the laboratory, including organic synthetic polymers, biomacromolecules or natural biopolymers, modified biopolymers, blends, inorganic/polymer nanocomposites, and ceramics. Electrospun fibrous structures have unique properties due to the biomimetic characteristics with fiber diameter in the nano-to-submicrometer range, high surface area-to-volume ratio, high interconnected porosity with tunable pore size, possibilities for surface functionalization, and structural similarity to the extracellular matrix. These characteristics make them good candidates for many technological applications such as filter, barrier and catalytic industrial products, intelligent clothing, energy storage, batteries, aerospace technology and biomedical devices among others [2,3]. Intrigued by the biomimetic structure of electrospun membranes, many researchers are studying its potential use as scaffolds for tissue engineering and drug delivery applications [4–7].

The development of tissue-engineered microvascular prostheses is still a challenge, and many approaches are currently being investigated [8]. Biopolymers such as collagen and elastin have been used to engineer vascular constructs [9,10]. However, their utility has been limited by poor mechanical properties and dimensional instability causing shrinkage and premature dissolution in culture conditions [11]. Functional vascular substitutes were also fabricated by electrospinning by using natural and synthetic polymer blends that mimic the extracellular matrix and mechanical properties of native blood vessels [12].

To mimic the mechanical behavior of natural arteries the vascular grafts diameter should present a "J" shaped response to pressure [13]. The collagen and elastin components in the arterial wall are responsible for this behavior; each natural polymer plays a different role. At high pressures collagen high modulus and stiffness supports the solicitations. At lower pressures, it is the elastin that dominates the mechanical response [14,15]. Elastin has a lower modulus and a viscoelastic response. Therefore, in order to obtain a successful vascular graft with biomimetic mechanical behavior a viscoelastic and a non-elastic material should be employed.

* Corresponding author at: INTEMA (UNMdP-CONICET), Av. Juan B. Justo 4302, B7608FDQ, Mar del Plata, Argentina. Tel.: +54 223 4816600#291.
E-mail addresses: florenciamontini@fi.mdp.edu.ar (F. Montini Ballarin), pcaracciolo@fi.mdp.edu.ar (P.C. Caracciolo), eblotta@fi.mdp.edu.ar (E. Blotta), vballari@fi.mdp.edu.ar (V.L. Ballarin), gabraham@fi.mdp.edu.ar (G.A. Abraham).

http://dx.doi.org/10.1016/j.msec.2014.05.074
0928-4931/

Poly(L-lactic acid) (PLLA) is a FDA approved biodegradable polyester commonly used in biomedical applications, such as drug delivery systems, tissue engineering, and biomedical devices that exhibit semicrystalline structure and good electro-spinnability [16–19]. PLLA possesses high elastic modulus required to withstand high pressure and flow without collapse or degradation until tissue develops and matures in vivo. PLLA has a mechanical response similar to collagen [20].

Segmented polyurethane (SPU) elastomers consisting of alternating soft and hard segments are generally thermoplastic with excellent physical properties, such as tensile strength, good compliance, and biocompatibility [21,22]. SPUs have been used in cardiovascular devices for almost 50 years [23]. Considering their superior physical properties principally their viscoelastic compliant nature, SPU provides the elastin-like mechanical behavior [24,25] for use in bypass procedures. Annis et al. were the pioneers in studying elastomeric vascular prosthesis obtained by electrospinning of poly(ether urethane) [26] and poly(ether urethane urea) [27]. Other vascular grafts prepared by electrospinning of biostable polyurethanes were also reported [28,29]. However, non-degradable polymers lack the ability to promote native tissue regeneration. Then, bioresorbable SPUs with non-toxic degradation byproducts are preferable for tissue engineered applications [30]. Still to these days there are not commercially available bioresorbable segmented poly(ester urethane)s (SPEU) nor poly(ester urethane urea)s, being only synthesized in a laboratory scale. Some research groups have reported electrospun scaffolds from bioresorbable SPEU [30–33].

To the best of our knowledge the development of bilayered vascular graft using of a novel biodegradable segmented poly(urethane) blended with PLLA in two different compositions, each of them mimicking the collagen-elastin ratio presented in the media and adventitia layers of natural arteries respectively, has not been reported before.

The present study is focused on the electrospinning process as a versatile technique to obtain nanofibrous structures. Although electrospinning is claimed in the literature as a simple technique, many parameters such as processing parameters and intrinsic properties of solutions should be carefully optimized in order to obtain uniform fibers with reproducible morphology. A bilayered tubular construct composed of PLLA/SPEU 50/50 blend (inner layer) and PLLA/SPEU 90/10 blend (outside layer) obtained by multilayering electrospinning is described in this work. Polymer blend ratios were chosen to mimic the media and adventitia layers [34]. The influence of the different electrospinning parameters into the fiber formation and fiber mean diameter for PLLA, SPEU and PLLA/SPEU blends were studied. Electrospinning parameters were optimized by using a regular flat collector. Flat and two-parallel plate collectors were used to analyze the effect of the electrostatic field on PLLA nanofiber alignment on a rotating mandrel. Finally, composition, surface hydrophilicity, thermal properties and morphology of nanofibrous scaffolds were characterized and discussed. Degradation behavior and biomechanical properties, in particular dynamic compliance under physiologic conditions, are under progress and will soon be published elsewhere.

2. Materials and methods

2.1. Materials

PLLA (PLA2002D Mw = 287.9 kg mol-1) was obtained from Natureworks (MN, USA). A bioresorbable SPEU named PHD was synthesized in our laboratory. Dichloromethane (DCM) and *N,N*-dimethylformamide (DMF) were acquired from Anedra (BA, Argentina). Tetrahydrofuran (THF) was purchased from Cicarelli (Santa Fé, Argentina). 2,2,2-trifluoroethanol (TFE) was purchased from Sigma-Aldrich (MO, USA). All solvents were analytical grade and were used as received.

2.2. Methods

2.2.1. Synthesis of segmented poly(ester urethane)

SPEU was synthesized from aliphatic diisocyanate, aliphatic polyester, and a novel aromatic chain extender according to previously reported procedures [25]. Briefly, PCL diol (Mn = 2.250 kg mol^{-1}) was prepared by ring opening polymerization of ε-caprolactone initiated by triethylene glycol. A tyrosine derivative was used as diester–diphenol chain extender. This compound was synthesized by a Fischer esterification reaction between 3-(4-hydroxyphenyl)propionic acid (desaminotyrosine) and ethylene glycol (2:1 mole ratio) catalyzed by *p*-toluene sulfonic acid in refluxing toluene. The reaction was driven toward completion by using a Dean-Stark apparatus to trap the evolved water.

SPEU was obtained by a two-step polymerization method. Briefly, PCL diol was reacted with HDI in a 1:2.01 molar ratio at 80 °C in anhydrous *N,N*-dimethylacetamide (DMAc) under stirring and nitrogen atmosphere. The prepolymerization proceeded in the presence of dibutyltin dilaurate as catalyst (0.1 wt.% of macrodiol) for 1 h, and then the solution was concentrated. The chain extender was previously dissolved in DMAc, and added at a molar ratio 1:1 with respect to the prepolymer. Chain extension reaction proceeded for 6 h at 80 °C. The resulting slurry was precipitated over cold distilled water. Then, the polymer was washed and dried under vacuum. Intrinsic viscosity [η] measurements by means of an Ubbelohde Type OC viscosimeter (Cannon) using DMAc as solvent at 30 ± 0.1 °C yielded the value of [η] as 0.49 $dl.g^{-1}$.

2.2.2. Preparation of PLLA, SPEU and PLLA/SPEU electrospun nanofibrous membranes

In order to optimize the experimental processing conditions, a standard electrospinning setup was used. Several solvent mixtures, polymer concentrations, and electrospinning parameters were studied. Each of the as-prepared solutions was loaded into a standard 10 ml plastic syringe connected to a polyamide tube, attaching to the open end a blunt 18-gauge stainless steel hypodermic needle as a nozzle. The flow rate was controlled by using a programmable syringe pump (Activa A22 ADOX S.A., Argentina). A high-voltage power source (ES30P, Gamma High Voltage Research Inc.) was used to charge the solution by attaching the emitting electrode of positive polarity to the nozzle, and the grounding one to the aluminum collecting plate. All experiments were carried out at room temperature in a chamber having a ventilation system. The electrospun scaffolds were dried under vacuum at room temperature to fully eliminate the residual solvent, and finally stored in a desiccator.

An optimum electrospinning condition for PLLA was set based on its influence in the production of uniform bead-free nanofibers. DMF and DCM were chosen as solvents and used in a 25:75 and 40:60 ratio, respectively. The solution concentrations (C) for PLLA were 7, 10 and 15% wt/v. For each different polymer solution the electrospinning parameters were varied. The following experimental values were used: Voltage, *V*: 10, 12, 15 kV; needle-collector distance, *d*: 10, 12, 15 cm; flow rate, *f*: 1, 2 ml/h). Table 1 summarizes all the electrospinning conditions studied.

For PHD, different solutions were also used to optimize the experimental conditions to get a bead-free nanofibrous morphology. In this case, the choice of both composition and ratio of the solvent mixture used to solubilize the polyurethane was critical for the production of uniform nanofibers. In a first attempt PHD solutions 30% wt/v in DMF/THF with 50/50, 40/60, 60/40 ratios were used. PHD solutions 40% wt/v in DMF/THF (60/40), 20% wt/v in DMF/THF (40/60) and 20% wt/v in DMF/DCM (40/60 and 30/70) were also used. Finally, PHD solutions in TFE at 20 and 25% wt/v were employed. In all the cases the electrospinning processing parameters were varied ($f = 0.5$, 1 ml/h; $d = 10$, 15 cm; $V = 10$, 13, 15, 20 kV).

Once each polymer electrospinning optimum condition was fixed, polymer blends were tried. Since the potential use of these scaffolds is

Table 1
Electrospinning parameters studied for PLLA solutions.

f (ml/h)	*d* (cm)	*V* (kV)	PLLA 15% *DMF/DCM 25/75*	PLLA 10% *DMF/DCM 25/75*	PLLA 10% *DMF/DCM 40/60*	PLLA 7% *DMF/DCM 40/60*
1	10	10	X	X	X	X
1	10	12	X	X	X	X
1	10	15	X	X	X	X
1	12	10	X	X	X	X
1	12	12	X	X	X	X
1	12	15	X	X	X	X
1	15	10			X	X
1	15	12				X
1	15	15			X	X
2	10	10	X			X
2	10	12				X
2	10	15				X
2	12	10		X		X
2	12	12		X	X	X
2	12	15		X	X	X

for small-diameter vascular grafts, the muscular artery composition was taken into account for the blend polymer ratio selection. Scaffolds are configured to accommodate an intimal layer of vascular endothelial cells. Two polymer blend ratios were chosen to mimic the media and adventitia layers, which in this work correspond to the inner and outer layers of the tubular scaffold. Based on muscular arteries collagen/elastin ratio [35] and the studied amount of each of these natural polymers on their layers [36,37], two PLLA/PHD blend ratios were selected.

PLLA was chosen as a mechanically similar polymer to collagen, whereas the characteristic viscoelasticity of PHD resembles the elastin behavior. PLLA/PHD with 50/50 and 90/10 ratios were chosen for the inner and outer layer, respectively. TFE was selected as solvent. First, the blend was prepared considering the ratio of each optimized polymer solution; i.e.: 50% of PLLA 10% wt/v and 50% of PHD 25% wt/v in TFE for the inner layer and 90% of PLLA 10% wt/v and 10% of PHD 25% wt/v in TFE for the outer layer. These resulted in a total concentration of 17.5% wt/v and 11.5% wt/v for the inner and outer layer respectively. In a second approach, the total solution concentration was increased, and a ratio based on weight of each polymer was employed. Thus, the following values were used: 20% wt/v in TFE for the inner layer with PLLA/PHD 50/50 wt/wt and 15% wt/v in TFE for the adventitia with PLLA/PHD 90/10 wt/wt. The electrospinning parameters used were $f = 0.5$, 1 ml/h; $d = 15$ cm; $V = 13$ kV.

2.2.3. Alignment of PLLA nanofibers

A collector consisting of two-parallel electrodes was used to study the alignment of PLLA nanofibers in order to obtain a collagen-like structure. The already explored PLLA solution (10% wt/v in DMF/DCM 40/60) was used to optimize the electrospinning parameters for a well-aligned topography. The effect of the distance between the plates (*dp*) as well as *f*, *d*, and *V*, were studied. The values explored were $dp = 2$, 2.5, 3 cm; $f = 0.5$, 1 ml/h; $d = 15$ cm; $V = 13$, 15 kV.

2.2.4. Preparation of small-diameter nanofibrous tubular structures

A small-diameter rotating mandrel (5 mm diameter, 15 cm length) was used as nanofiber collector to obtain tubular structures. PLLA solution of 10% wt/v was electrospun at $f = 0.5$ ml/h, $d = 15$ cm, $V = 13$ kV, and rotation speed (r) = 1000 rpm. Flat and two-parallel plate collectors were separately placed under the rotating mandrel to analyze the effect of the electrostatic field on the fiber alignment within the tube. PHD 25% wt/v solution was electrospun at $f = 1$ ml/h, $d = 15$ cm, $V = 13$ kV, and $r = 1000$ rpm. A flat collector was used as auxiliary collector. For the inner and outer layers a solution of 20% wt/total volume of PLLA/PHD 50/50 wt/wt and 15% wt/total volume of PLLA/PHD 90/10 wt/wt were used, respectively. The electrospinning parameters used for the inner layer were the ones used for PHD and for the outer layer the ones used for the PLLA.

2.2.5. Characterization

2.2.5.1. Thermal properties. Differential Scanning Calorimetry (DSC) analysis of electrospun scaffolds was carried out with a Perkin-Elmer Pyris 1 instrument (Perkin-Elmer, USA), at a heating rate of 10 °C/min from −60 to 200 °C under nitrogen atmosphere. The glass transition, crystallization and melting temperatures, crystallization and melting enthalpies, and the possible changes in these thermal events due to the processing, were evaluated.

2.2.5.2. Fourier Transform Infrared Spectroscopy. Fourier Transform Infrared Spectroscopy (FTIR) spectra using attenuated total refractance (ATR) mode were recorded at room temperature using Nicolet 6700 (Nicolet Instruments Inc., WI, USA). FTIR spectra were obtained over a range of 450–4000 cm^{-1} at a resolution of 2 cm^{-1}.

2.2.5.3. Contact angle measurements. The contact angle of water droplets (5 μL) on dry membrane pieces was measured with a goniometer (Ramé-Hart Co; USA. 15 measures in 300 s) and analyzed by using the Ramé-Hart software.

2.2.5.4. Nanofiber morphology. Micrographs of the PLLA, PHD and PLLA/PHD blends membranes and tubular structures were recorded in a Scanning Electron Microscope (SEM) (JSM-6460LV; JEOL, Japan) after sputter coating with gold, and processed with image processing software (Image Pro Plus; Media Cybernetics Inc., USA). The diameter and orientation of 100 nanofibers per sample were measured in order to obtain a meaningful statistical value. A mathematical algorithm based in mathematical morphology techniques was used to measure the fiber alignment as well. This algorithm uses the size granulometric function to quantify the orientation of the nanofibers, and also performs a statistical analysis of each image morphology. Briefly, the normalized size granulometric distribution function (FGTN) (Eq. (1)) was defined from the resulting family of applying consecutive apertures with structural elements of crescent size, λ.

$$G(\lambda) = 1 - \Omega(A \circ E_\lambda)/\Omega(A) \quad (1)$$

where A is the aperture operation determined by the structural element E_λ and Ω is a measure of the resulting image. After determining the FGTN, which behaves as a probability distribution function, the mean value, standard deviation and energy of this function were obtained. These values were used as the image statistics. A linear structural element (with different orientations from 0° to 175°) was applied in correspondence with the nanofiber shape [38].

3. Results and discussion

3.1. Effect of solution properties on PLLA, PHD and PLLA/PHD blends fiber morphology

A complete study of the electrospinning parameters and their influence on the nanofiber diameter was made for PLLA. Three different polymer concentrations were explored (7, 10 and 15% wt/v). It was observed that the 7% wt/v concentration was below the critical concentration for the production of bead-free nanofibers. A mixed structure of fibers and some small beads was obtained (Fig. 1a). In the case of both 10% and 15% wt/v bead-free nanofibrous structures were observed (Fig. 1b, c). The 10% wt/v solution was chosen for being the one over the critical concentration required to produce polymer chain entanglements for fiber formation. Even more, this concentration resulted in smaller fiber mean diameter, as it was expected.

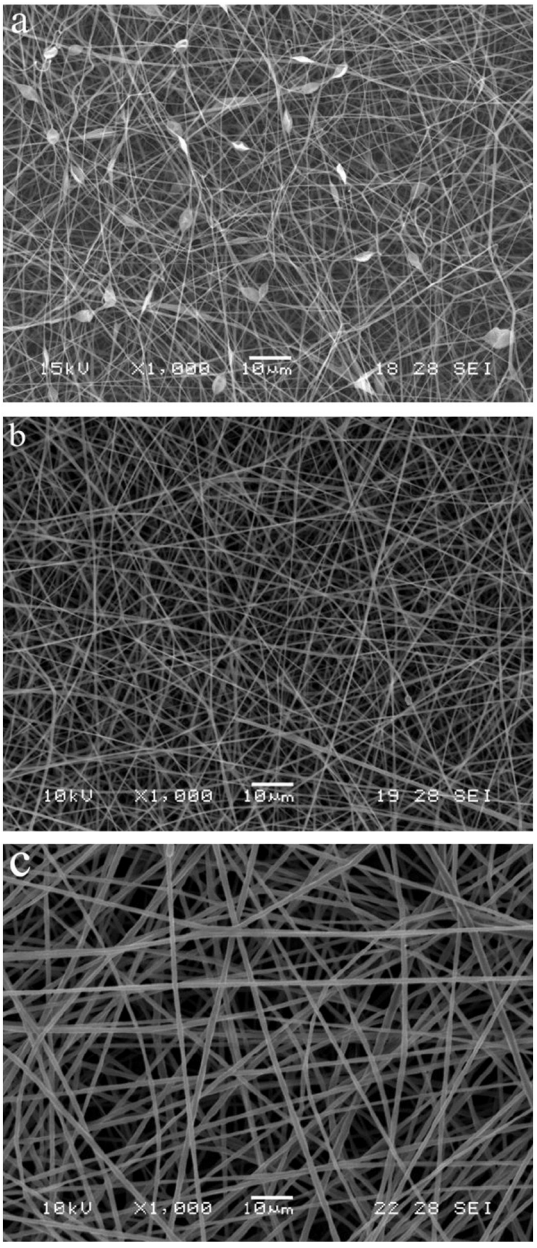

Fig. 1. SEM micrographs of PLLA electrospun membranes from 7% (a), 10% (b) and 15% (c) wt/v.

The effect of the solvent used was also analyzed by varying the DMF/DCM ratio between 25/75 and 40/60% v/v. During the electrospinning process the solvent evaporates almost completely in the trajectory of the jet toward the collector. Although it was expected to obtain a smaller fiber mean diameter from the solvent mixture containing the higher amount of the solvent with lower boiling point (DCM), the polar nature of DMF turns the solution into a more conductive one. Since the process is governed by a voltage difference, the higher driving force led to a decrease in the nanofiber diameter and standard deviation when DMF/DCM 40/60 was used.

The processing parameters (V, d, f) did not present a significant influence on the nanofibers mean diameter. The most meaningful of the three parameters was the flow rate. However, its effect on the nanofiber morphology was not as important as the one observed for the solution properties. It was observed that the increase in flow rate decreased the mean fiber diameter. However, it was evidenced that when the flow rate increased a broad size distribution was found. After this analysis the mean fiber diameter resulted in 506 ± 136 nm for a PLLA solution 10% wt/v in DMF/DMC 40/60 electrospun at $f = 1$ ml/h, $V = 10$ kV, and $d = 10$ cm.

For electrospinning PHD solutions, many solutions were tried and different morphologies were obtained. The most significant parameters in the process were solution properties, polymer concentration and solvent, so that these were the ones analyzed. Table 2 summarizes the morphological results. When mixtures of DMF, THF or DCM were used, a morphology of fused beads with few small connecting fibers was observed (Fig. 2a–b). It was hypothesized that, in these solvent mixtures, all solutions were below the polymer critical concentration for polymer chain entanglements needed for fiber formation. However, for higher concentration, the increase in solution viscosity prevented the process. After discharging the use of these solvents, TFE was selected as a candidate based on the literature reports in which 1,1,1,3,3,3-hexafluoro-2-propanol (HFP) was used as good solvent for some polyurethane formulations [30,32,33].

Due to the high cost of HFP, TFE was thought as a less expensive fluorinated solvent that could electrospun PHD. The solution of 20% w/v resulted in a beaded fibrous morphology (Fig. 2c). When the polymer concentration was increased to 25% wt/v a bead-free morphology was obtained (Fig. 2d). For this solvent–polymer system the critical concentration resulted lower than for the other systems.

The influence of some processing parameters (f, d, V) was studied. As in the case of PLLA, the most significant of these parameters was the flow rate. A higher flow rate produced smaller mean fiber diameter. PHD membranes mean fiber diameter was 581 ± 379 nm for a 25% wt/V TFE solution electrospun at $f = 1$ ml/h, $V = 13$ kV, and $d = 15$ cm.

After optimizing the experimental conditions for nanofiber formation from pure polymers, the best conditions for processing polymer blends were achieved. In a first study, solutions of 25% wt/v PHD in TFE and PLLA 10% wt/v in TFE were prepared, and a percentage by volume of each solution was mixed. For the inner layer a PLLA/PHD 50/50% v/v was used (Fig. 3b), whereas 90/10% v/v was used for the outer layer (Fig. 3a). A total concentration of 17.5% wt/v and 11.5% wt/v for the inner and outer layer respectively was used. SEM micrographs showed a beaded fiber morphology, with the outer layer presenting a higher amount of beads. The reason for this morphology was the use of a solution concentration below the critical value for bead-free fiber formation. Since the PLLA critical concentration of 10% wt/v corresponded to the mixture DMF/DMC it could be thought that for

Table 2
SPEU solutions studied and morphology results.

Sample	Solution concentration and solvent mixture (v/v)	Fiber morphology
1	30% wt/v in DMF/THF = 50/50	No fibers: fused beads with small fibers tying them together
2	30% wt/v in DMF/THF = 40/60	No fibers: fused beads into thick fibers and spheres
3	30% wt/v in DMF/THF = 60/40	No fibers: beads with a few small fibers tying them together
4	40% wt/v in DMF/THF = 60/40	No fibers: disperse beads with a few small fibers tying them together
5	20% wt/v in DMF/THF = 40/60	No fibers: beads with a few small fibers tying them together
6	20% wt/v in DMF/DCM = 40/60	No fibers: fused beads with small fibers tying them together
7	20% wt/v in DMF/DCM = 30/70	No fibers: fused beads with a few small fibers tying them together
8	20% wt/v in TFE	Beads and fibers
9	25% wt/v in TFE	Random fibers

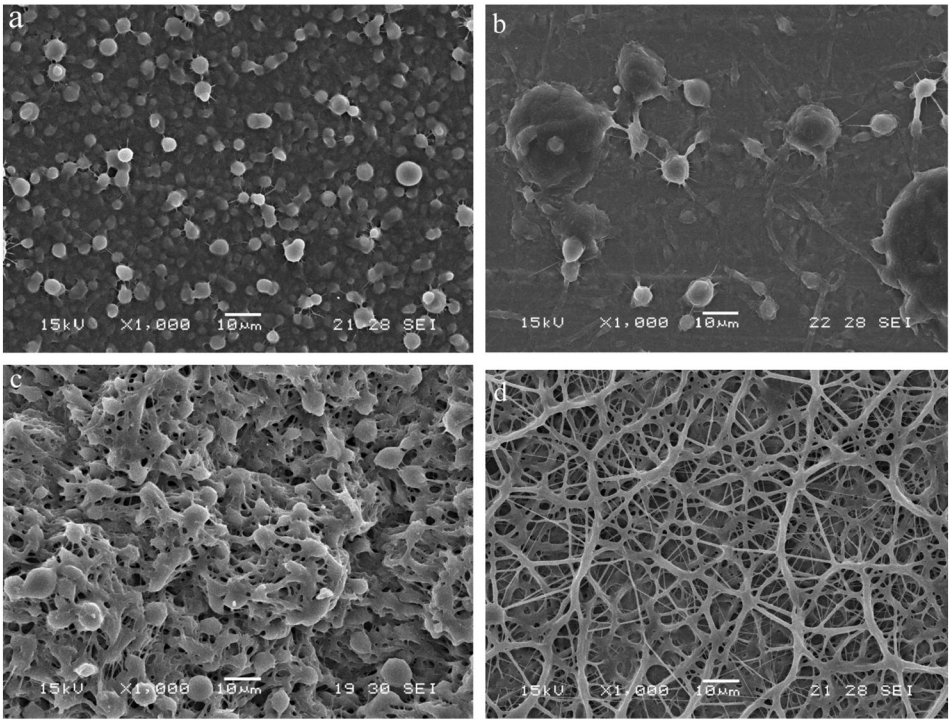

Fig. 2. SEM micrographs of the PHD membranes obtained from 30% wt/v in DMF/THF = 60/40 (a), 30% wt/v in DMF/THF = 40/60 (b), 20% wt/v in TFE (c) and 20% wt/v in TFE (d).

the TFE this concentration should be higher. This agrees with the fact that the blend with higher percentage of PLLA (outer layer) exhibited more beads. In order to obtain nanofibrous structure, blends were prepared by using weight ratios, keeping the same percentage as for volume ratios and raising the polymer total concentration from 11.5% wt/v and 17.5% wt/v to 15% wt/v and 20% wt/v for inner and outer layers, respectively. With the increase in the global concentration bead-free uniform nanofibrous structures were obtained (Fig. 4c, d). This analysis confirms that the solution concentration and solvent used are the more significant variables in the electrospinning process of these polymer systems. Again, some processing parameters were varied and the result showed that the flow rate had a meaningful influence, especially for the outer solution for which a higher flow rate resulted in a beaded structure.

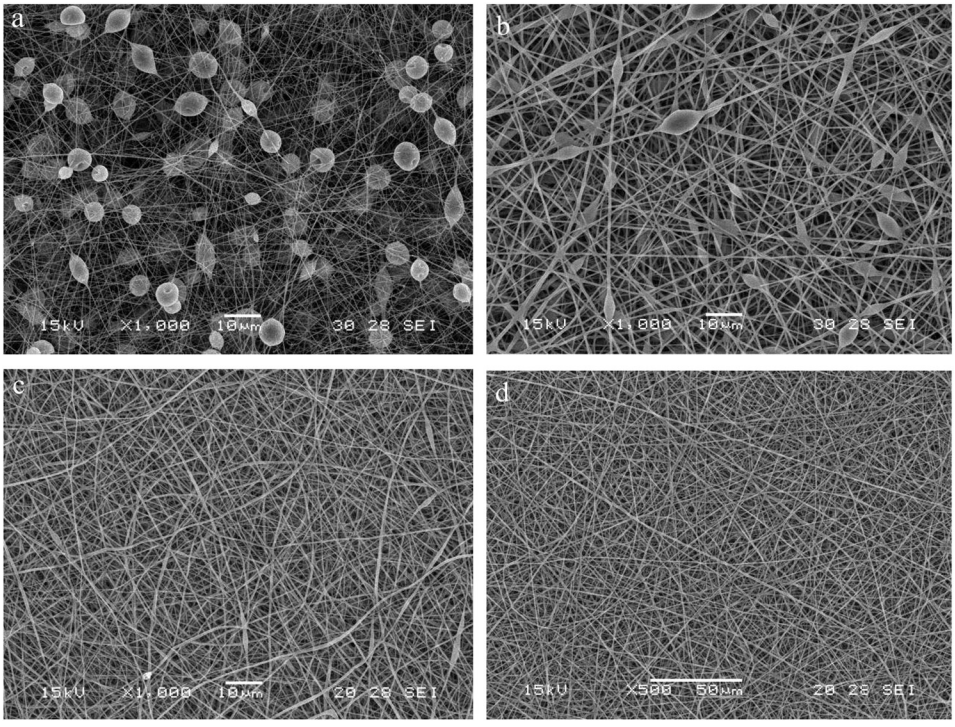

Fig. 3. SEM micrographs of the outer layer from blend based on volume ratio (a), inner layer from blend based on volume ratio (b), outer layer from blend based on weight ratio (c) and inner layer from blend based on weight ratio (d).

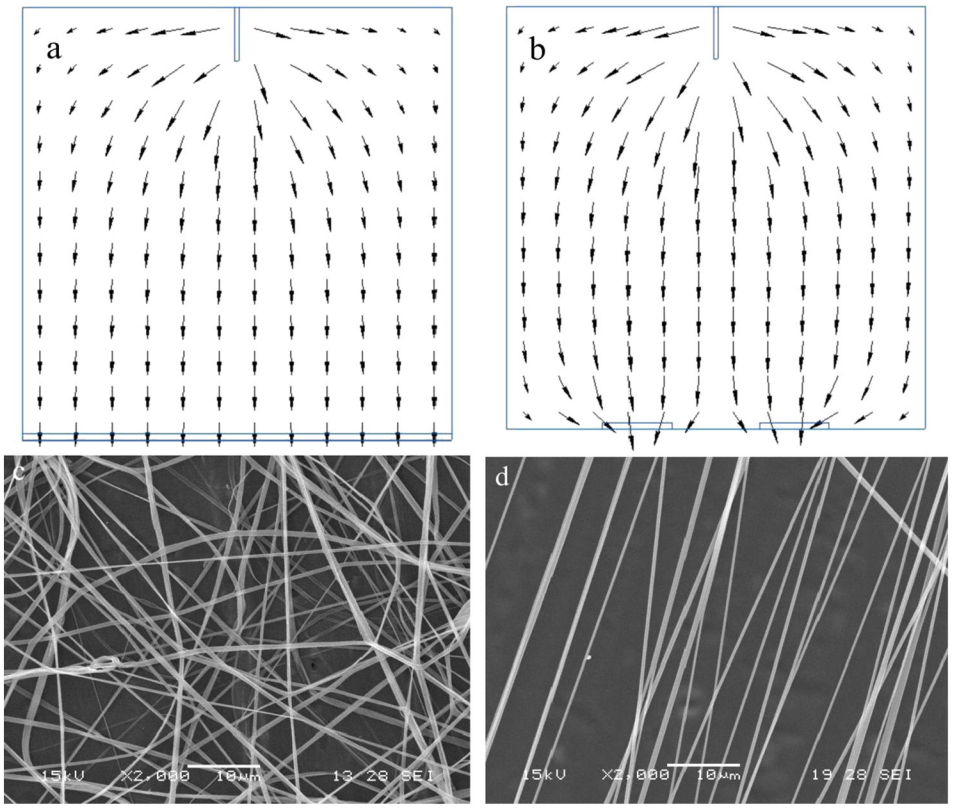

Fig. 4. Electrical field lines modeled by finite elements for (a) plate and (b) two-parallel plate collectors. SEM micrographs of membranes obtained when (c) a plate and (d) two-parallel plate collectors, were used.

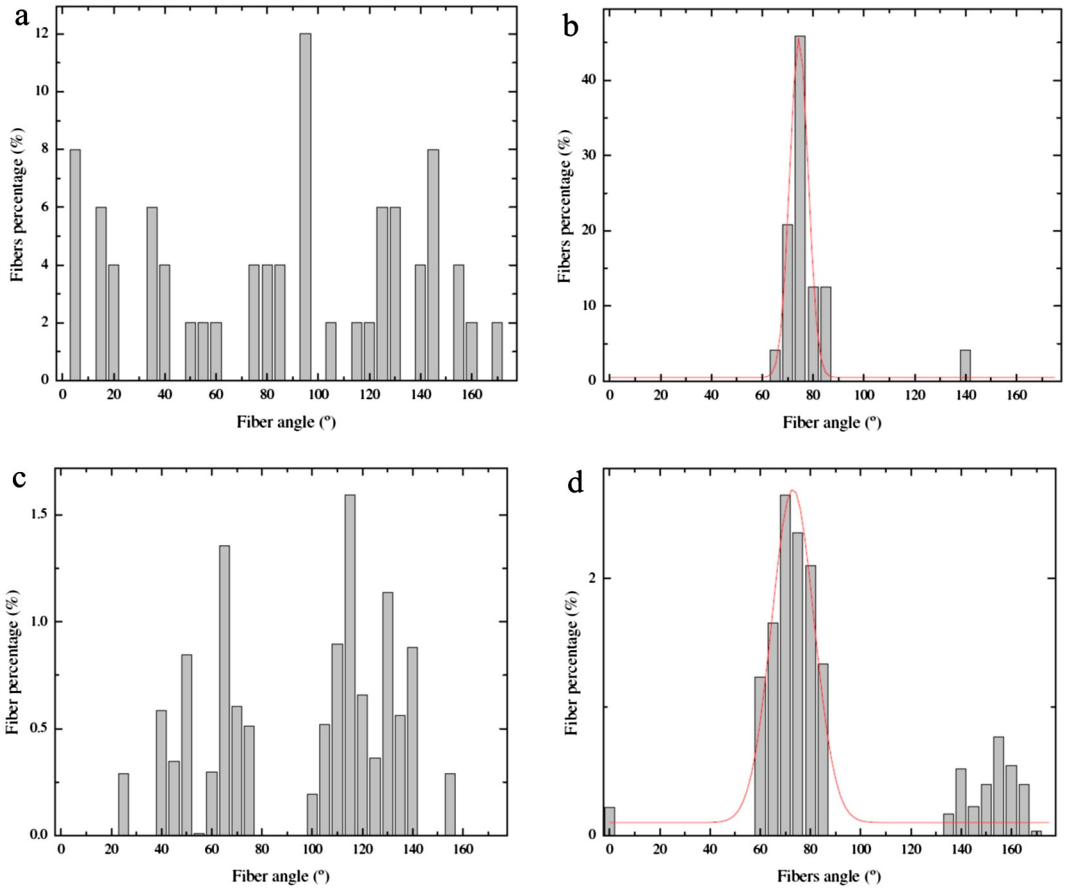

Fig. 5. Histograms corresponding to random (a, c) and aligned (b, d) membranes as obtained by IP (a, b); and MA (c, d) image processing techniques.

The optimal electrospinning conditions were 20% wt/v PLLA/PHD 50/50 wt/wt electrospun at $f = 1$ ml/h, $V = 13$ kV, and $d = 15$ cm and 15% wt/v PLLA/PHD 90/10 wt/wt electrospun at $f = 0.5$ ml/h, $V = 13$ kV, and $d = 15$ cm for the inner and outer layers, respectively. These conditions produced bead-free unimodal nanofibers with a mean diameter of 327 ± 116 nm for the adventitia layer and 570 ± 162 nm for the media.

3.2. Effect of auxiliary collectors on fiber alignment

In natural blood vessels there are preferential collagen fiber orientations in the outer layer (adventitia), which provide successfully concentrically contraction and dilatation during diastolic and systolic cycle [39]. In this way nanofiber orientation could favor the compliance match. Besides, a preferential nanofiber orientation could benefit cell differentiation, proliferation and functional longevity in tissue engineering scaffolds. Therefore, it is important to mimic the collagen aligned topography on natural arteries external layer. For this reason, the effect of placing a grounded parallel-plate collector on dividing the electric field and the resulting nanofibrous topography was analyzed. The PLLA solution optimized by using a flat collector (10% wt/v DMF/DCM 40/60) was used to obtain aligned nanofibers. Processing parameters such as flow rate, needle-collector distance, voltage and distance between plates were varied. The degree of alignment was analyzed by manual image processing (IP) measurements and the mathematical algorithm based in mathematic morphology techniques (MA) (Section 2.2.5.4). Again, the flow rate showed the most significant effect on the nanofibrous topography. A value of $f = 1$ ml/h produced random oriented nanofibers. Other parameters, like voltage or distance between plates influenced the degree of alignment but all samples processed with $f = 0.5$ ml/h exhibited aligned nanofibers.

Fig. 4a–b showed the electrical field lines for both collectors as modeled by finite elements. It can be appreciated that the field is divided into two when the parallel-plate collector was used. Fig. 4c–d displays the topography difference that resulted from each collector, obtaining random and aligned oriented nanofibers respectively. Electrospinning at $f = 0.5$ ml/h, $d = 15$ cm, $V = 13$ kV, *d-plates* = 2.5 cm produced a well-aligned nanofibrous membrane with a mean fiber angle of 75 ± 14.21° (IP) and 82.87 ± 27.59° (MA). The mean fiber angle of Fig. 4c was 79 ± 53.05° (IP) and 96 ± 35.08° (MA). Fig. 5 presents the fiber angle histogram of both Fig. 4c–d. Even though there is a difference up to 20° [38], which was more marked for random topography, the histograms presented good agreement between both techniques. The software was a faster instrument to measure the membrane topography which resulted in good agreement with the tedious manual measurements.

PLLA membrane nanofiber mean diameter was affected by the change in electrospinning parameters in order to benefit the alignment topography. A mean diameter of 514.34 ± 163.10 nm was obtained.

3.3. Small-diameter tubular structures

Once the electrospinning conditions were optimized by using flat and parallel-plate collectors, tubular nanofibrous structures were obtained by using a 5-mm diameter rotating collector. Fig. 6 shows the macro and micrographs of PLLA and PHD tubular structures. Nanofibrous

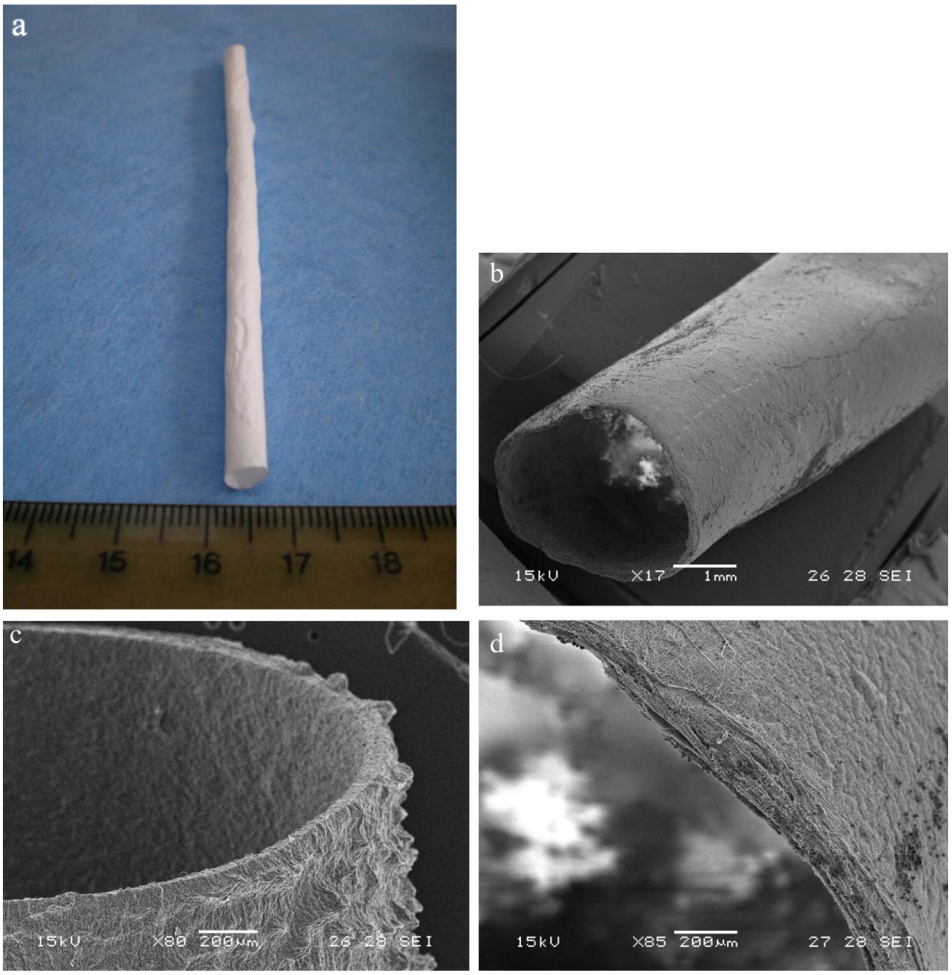

Fig. 6. Digital photograph (a) and SEM micrographs of PLLA (b), (d) and PHD tubular nanofibrous structures (c).

three-dimensional tubular structures with no welds were obtained. The rotating collector did not affect the nanofibrous morphology, neither for the pure polymers nor their blends. PLLA nanofibers displayed a 383 ± 103 nm mean diameter. A mean fiber diameter slightly higher was obtained for PHD, inner and outer layer tubular samples; the structures presented a value of 687 ± 290 nm, 754 ± 210 nm and 410 ± 124 nm, respectively.

A bilayer tubular scaffold was obtained by sequential electrospinning. First the inner layer solution was electrospun over the rotating collector; this was followed by the outer layer deposition. The final graft did not show delamination which reflects a good adhesion between both layers. Mechanical characterization of the bilayer grafts is being conducted at the moment.

In the case of PLLA tubular structure an auxiliary parallel-plate collector was used under the rotating collector to separate the field and obtain an aligned topography. The studied conditions for aligned membranes with the parallel-plate collector were used.

Again, the degree of alignment was measured by IP and MA image processing techniques. Mean angles of 114 ± 26.2° (IP) and 109 ± 34.2° (MA) were obtained. Fig. 7 presents the topography on the tubular surfaces and the angle histograms measured by both techniques. Although due to the size of the standard deviation this cannot be called as aligned topography, the SEM micrograph reveals some degree of fiber orientation. It can be appreciated that both techniques resulted in a mayor angle around 110°, which corresponds to the direction of the small orientation present in Fig. 7a. Some degree of alignment was obtained in the surface structure as it was expected, and in accordance with literature [39], due to the electrical field separation.

3.4. Nanofiber characterization

Tubular structures were analyzed by FTIR to observe the polymer composition (Fig. 8). In Fig. 8(d) all characteristic bands of PLLA could be observed (methyl, carbonyl ester, and alkyl groups). In the case of PHD, the presence of urethane groups was observed at 3368 cm^{-1} (νN-H band), and as a shoulder at 1680–1686 cm^{-1} (carbonyl–urethane amide I band). These urethane groups connect the hard and soft segments. The spectra of blends (Fig. 8a, b) showed, as expected, the presence of both polymers. The outer layer presented predominantly the common bands for both polymers, being more intense the ones for PLLA (PLLA/PHD 90/10). The wider right end of the band at 1686 cm^{-1}, as well as the weak methylene band at 2865 cm^{-1}, both absent in PLLA were associated to PHD. The inner layer spectrum showed more clearly the characteristic bands of both polymers. The urethane band at 3368 cm^{-1} along with more pronounced bands at 1686 cm^{-1} and 2865 cm^{-1} characteristic for PHD were observed. Moreover, both carbonyl ester bands (for PLLA and PHD) could also be seen.

Thermal properties of electrospun samples were studied by DSC. Fig. 9 displays the thermograms. Two effects could be appreciated by analyzing the curves: the influence of the electrospinning process and the polymer blend on the thermal properties of the samples.

Table 3 shows the glass transition temperature (T_g), crystallization temperature (T_c), melting temperature (T_m), crystallization and melting enthalpies (ΔH_c and ΔH_m) and crystallinity percentage (Xc) of raw PLLA

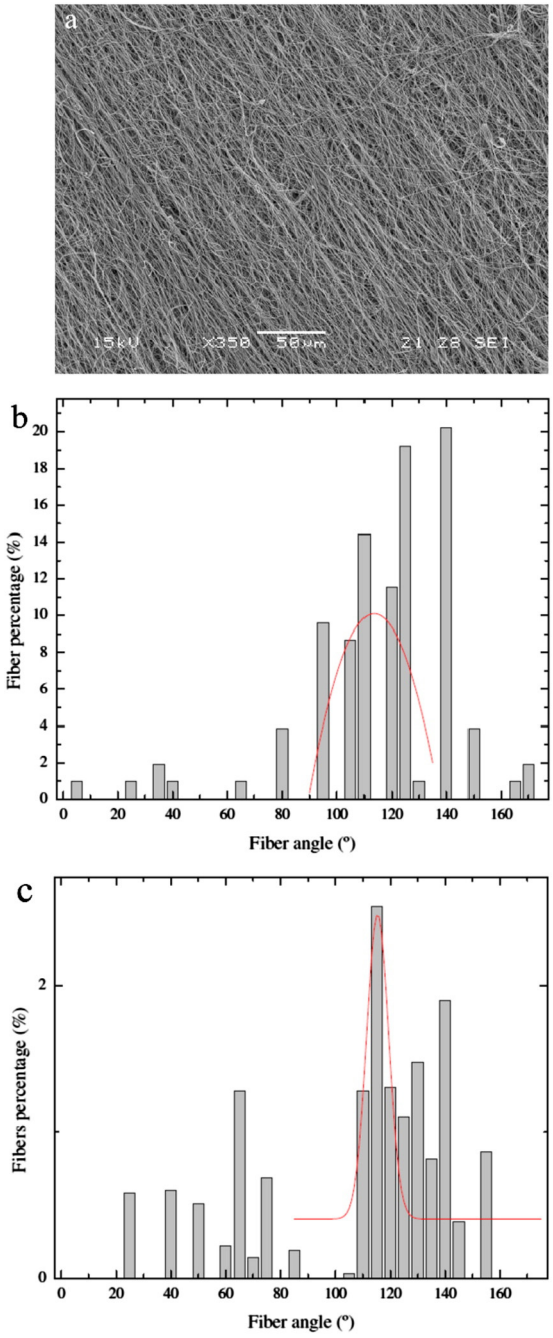

Fig. 7. SEM micrograph of PLLA tubular nanofibrous structure surface (a), and its angle histogram measured by IP (b) and MA (c).

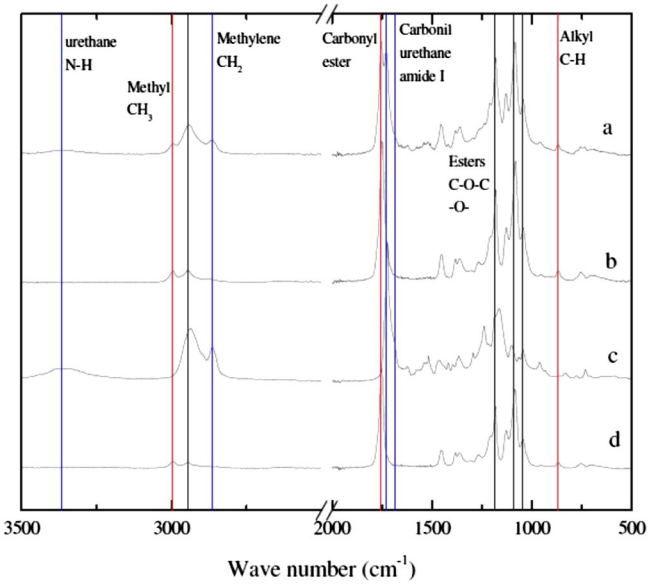

Fig. 8. ATR-FTIR spectra of inner layer blend (a), outer layer blend (b), PHD (c), and PLLA (d).

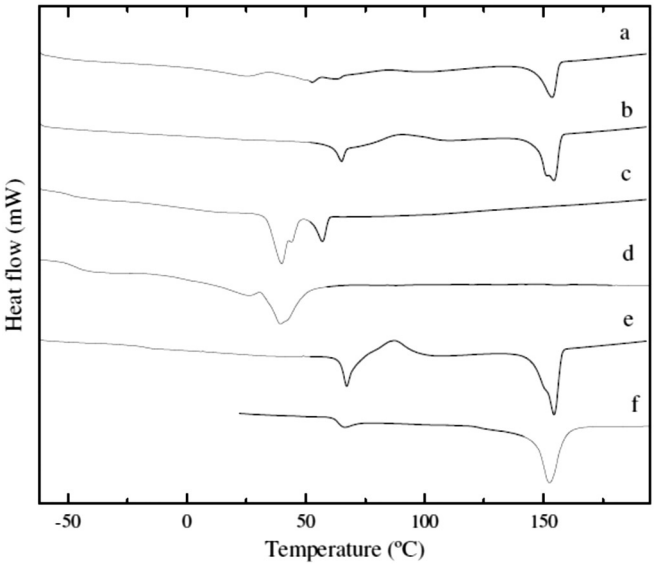

Fig. 9. DSC thermograms of electrospun inner layer blend (a), outer layer blend (b), electrospun PHD (c) and PLLA (e), and raw polymers PHD (d) and PLLA (f).

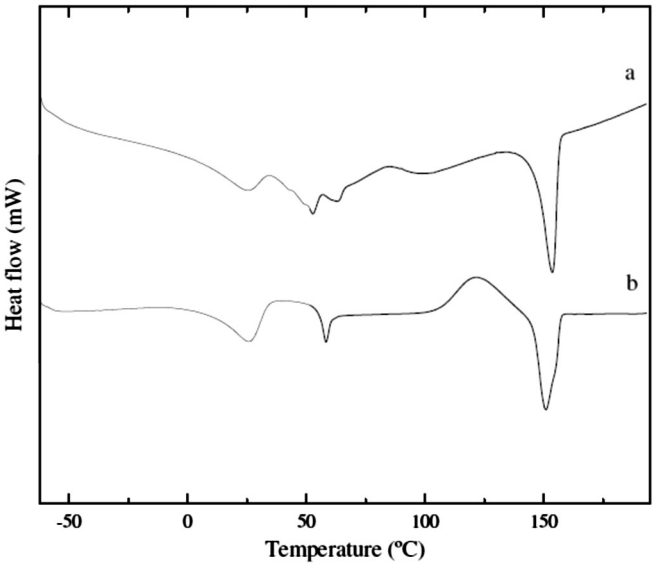

Fig. 10. DSC thermograms of inner layer, first (a), and second (b) scans.

and PHD, and electrospun PLLA, PHD, outer and inner blends. The subscript 's' on the PHD thermal events refers to the soft segment properties; thermal transitions of the hard segment were not detected by DSC.

By comparing the thermal properties of raw PLLA and its electrospun sample it can be appreciated that neither the glass transition nor the melting temperature were modified by the electrospinning process. These values were close to the one found in literature. The main change introduced by the processing of the PLLA is the decrease in the polymer crystallinity. This fact is due to fast solidification of the polymer, inhibiting the chains arrangement, getting this way a higher amorphous phase [42].

The thermal analysis of PHD casted film was reported by Caracciolo et al. [25]. When comparing film and electrospun PHD, it was observed that the $T_{g,s}$ value was not modified by the electrospinning process. The electrospun sample showed three peaks associated with the melting of soft domains at higher temperatures than those reported for the film. X_c was higher for the electrospun sample than the film; this phenomenon is hardly found in the literature. The presence of a higher fraction of crystals with a higher degree of order is difficult to explain in terms of intermolecular interactions. Zhuo et al. [43] also observed higher crystallinity in SPEU nanofibers with shape memory, and they attributed this fact to a positive tropism of the soft segment. The polymer did not show thermal transitions associated with hard domains, and this could be attributed to the fact that large chain extenders make difficult the ordering that leads to the crystallization of hard segments. Therefore, the composition and structure of chain extenders have significant effects on the thermal behavior and the processing method.

The thermogram of the outer layer blend only presents the thermal effects corresponding to PLLA, due to the small percentage of PHD in the blend (only 10% wt/wt). However, the increase in PLLA crystallinity could be attributed to PHD presence. All other thermal parameters did not seem to be influenced sustainably. The inner layer thermogram showed some overlapping events. Since the T_m of PHD soft segments is close to the T_g of PLLA, a second heating was performed to separate these thermal events. Fig. 10 presents both curves. As it could be appreciated, T_g of PLLA was overlapped with PHD soft segment melting peaks. The T_g PLLA value was obtained from the second heating curve, whereas the crystallinity of PHD soft segments and PLLA was calculated from the first scan since these events change during the second heating. The spectrum presents the thermal events of both polymers. The blending with PHD influenced both PLLA and PHD thermal properties. It was found that the addition of soft components, like poly(ethylene oxide), to PLLA can act as a plasticizer [44]. The smaller molecular weight PHD could act as a plasticizer for PLLA, which explained the decrease in T_g of PLLA. The T_g of PHD was not completely visualized; a drop could be seen at −59 °C that was attributed to T_g of PHD. Neither the melting nor the crystallization temperatures of the polymers were affected by the blend. The crystallinity degree, on the other hand, was different than the one for the pure electrospun polymers. In the case of PLLA, an increase in the polymer crystallinity was observed. A common defect of the PLLA plasticizers is the migration of plasticizer molecules to the surface induced by the crystallization of PLLA and phase separation [45]. In fact, the increase in the crystallization degree of PLLA has been reported for blends with poly(ε-caprolactone), which is the component of the soft segments of PHD [46]. On the other hand, PHD presented a decrease of its soft segment crystallinity degree. This effect could be caused by the long PLLA chains which make difficult the movement of PHD chains and make it more difficult for its soft segments to crystallize. As a result, both polymers present a lower crystallinity degree in the electrospun blends than in raw films. This could favor their mechanical properties and hydrolytic degradation, making them more attractive to

Table 3
Thermal properties of raw PLLA, PHD, and electrospun PLLA, PHD, inner and outer blends.

Sample	T_g PLLA (°C)	$T_{g,s}$ PHD (°C)	T_c PLLA (°C)	ΔH_c PLLA (J/g)	T_m PLLA (°C)	ΔH_m PLLA (J/g)	X_c PLLA[a] (%)	$T_{m,s}$ PHD (°C)	$\Delta H_{m,s}$ PHD (J/g)	X_c PHD[b](%)
PLLA raw	61.4	–	–	–	152.5	35	37.6	–	–	–
PHD film		−53.2	–	–	–	–	–	26.6, 39.3	29.8	26.4
PLLA	63.6	–	87.2	19.3	154.5	33.0	14.8	–	–	–
PHD	–	−51.6	–	–	–	–	–	39.9, 43.9, 57.0	40.9	36.2
Outer layer	61	–	90.2	14.7	151.6, 154.4	29.8	16.3	–	–	–
Inner layer	55	−59	83.4	9.1	153.7	33.6	26.4	25.0, 49.2, 52.7	18.5	16.4

[a] The degree of crystallinity (Xc) for PLLA was calculated considering 93 J/g as ΔH_m for PLLA 100% crystalline [40].
[b] Xc of PHD was calculated considering 148.05 J/g as ΔH_m for pure high-molecular-weight PCL (PHD soft domains) [41].

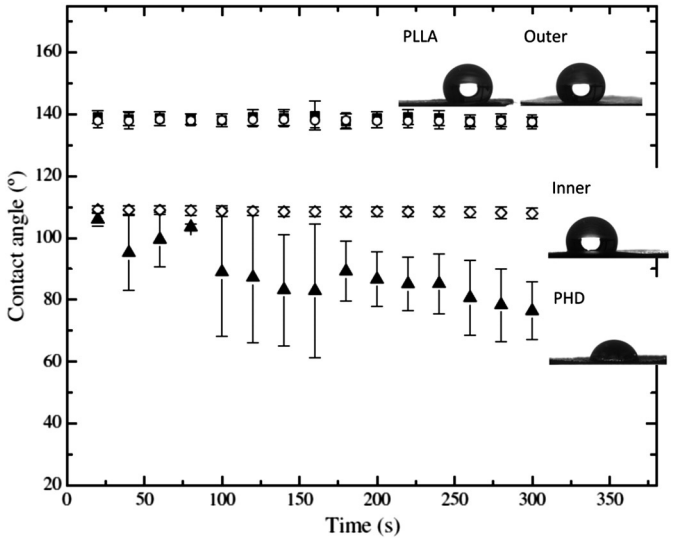

Fig. 11. Contact angle measurements as a function of time for electrospun PLLA (■), outer layer (○), inner layer (◊) and PHD (□).

tissue engineering applications. The thermal behavior of blends showed that the polymers are not miscible in each other, however the amorphous part of each could be partially miscible.

The contact angle of the electrospun samples was measured. Fig. 11 presents the angle as a function of time for the electrospun samples. PLLA presented a typical hydrophobic behavior with a contact angle around 140°. PHD showed a variable contact angle with time, it went down from 100° to 76° after 5 min. It was observed that after 5 more minutes the drop was absorbed completely. Therefore, electrospun PHD displayed a hydrophilic behavior. The values for blends were the expected ones. The outer layer, which is in its majority PLLA, presented a contact angle slightly under 140°. The inner layer showed a contact angle value in between the pure polymer values. These results showed that PLLA hydrophobic behavior was reduced by the blend with PHD. The inner layer is the one where a layer of endothelial cells will be cultured to obtain the intima layer, and the one that needs higher hydrophilicity.

4. Conclusions

The electrospinning parameters and solution intrinsic properties were optimized for PLLA, a bioresorbable segmented polyurethane, and their blends. Bead-free uniform nanofibers were obtained. Membrane topography was varied by electrical field separation; conditions for parallel-plate collector were also optimized. Membrane topography resulted in random or aligned nanofibrous structures depending on the auxiliary collector setup used. Tubular nanofibrous structures were produced by using a rotating collector. A bilayered vascular graft was successfully produced by sequential electrospinning of the blends solutions. Electrospun blends exhibited better thermal, physical and surface properties than raw polymers. The prepared scaffolding tubular structures are promising candidates for vascular tissue engineering as bilayered vascular grafts. The blends presented lower crystallinity degree than raw materials which suggests a faster hydrolytic degradation (studies under progress).

Acknowledgments

F.M.B. thanks CONICET for the fellowship awarded. This work was supported by the Argentinean National Agency of Scientific and Technological Promotion (PICT 448 grant), the National Research Council (PIP 522 grant), and the National University of Mar del Plata (15/G359 and 15/G328 grants).

References

[1] A. Greiner, J.H. Wendorff, Electrospinning: a fascinating method for the preparation of ultrathin fibers, Angew. Chem. Int. 46 (2007) 2–36.
[2] P. Raghavan, D.-H. Lim, J.-H. Ahn, Ch. Nah, D.C. Sherrington, H.-S. Ryu, H.-J. Ahn, React. Funct. Polym. 72 (2012) 915–930.
[3] S. Agarwal, A. Greiner, J.H. Wendorff, Functional materials by electrospinning of polymers, Prog. Polym. Sci. 38 (2013) 963–991.
[4] M. Zamani, M.P. Prabhakaran, S. Ramakrishna, Advances in drug delivery via electrospun and electrosprayed nanomaterials, Int. J. Nanomedicine 8 (2013) 2997–3017.
[5] R.L. Dahlin, F. Kurtis Kasper, A.G. Mikos, Polymeric nanofibers in tissue engineering, Tissue Eng. Part B 17 (2011) 349–364.
[6] S. Agarwal, J.H. Wendorff, A. Greiner, Use of electrospinning technique for biomedical applications, Polymers 49 (2008) 5603–5621.
[7] T.J. Sill, H.A. von Recum, Electrospinning: applications in drug delivery and tissue engineering, Biomaterials 29 (1989–2006) 2008.
[8] V. Vindigni, G. Abatangelo, F. Bassetto, New developments in tissue engineering microvascular prostheses, in: R. Pignatello (Ed.), Biomaterials Science and Engineering, Intech, Croatia, 2011, pp. 423–436.
[9] S.A. Sell, P.S. Wolfe, K. Garg, J.M. McCool, I.A. Rodriguez, G.L. Bowlin, The use of natural polymers in tissue engineering: a focus on electrospun extracellular matrix analogues, Polymers 2 (2010) 522–553.
[10] M. Li, M.J. Mondrinos, M.R. Gandhi, F.K. Ko, A.S. Weiss, P.I. Lelkes, Electrospun protein fibers as matrices for tissue engineering, Biomaterials 26 (2005) 5999–6008.
[11] Y. Hiraoka, Y. Kimura, H. Ueda, Y. Tabata, Fabrication and biocompatibility of collagen sponge reinforced with poly(glycolic acid) fiber, Tissue Eng. 9 (2003) 1101–1112.
[12] S.J. Lee, J. Liu, S.H. Oh, S. Soker, A. Atala, J.J. Yoo, Development of a composite vascular scaffolding system that withstands physiological vascular conditions, Biomaterials 29 (2008) 2891–2898.
[13] H.S. Rapoport, J. Fish, J. Basu, J. Campbell, C. Genheimer, R. Payne, D. Jain, Construction of a tubular scaffold that mimics J-shaped stress/strain mechanics using an innovative electrospinning technique, Tissue Eng. Part C 18 (2012) 567–574.
[14] R.L. Armentano, J.G. Barra, J. Levenson, A. Simon, R.H. Pichel, Arterial wall mechanics in conscious dogs: assessment of viscous, inertial, and elastic moduli to characterize aortic wall behavior, Circ. Res. 76 (1995) 468–478.
[15] M.A. Lillie, T.E. Armstrong, S.G. Gérard, R.E. Shadwick, J.M. Gosline, Contribution of elastin and collagen to the inflation response of the pig thoracic aorta: assessing elastin's role in mechanical homeostasis, J. Biomech. 45 (2012) 2133–2141.
[16] J.D. Roh, G.N. Nelson, M.P. Brennan, T.L. Mirensky, T. Yi, T.F. Hazlett, G. Tellides, A.J. Sinusas, J.S. Pober, W.M. SAltzman, T.R. Kyriakides, C.K. Breuer, Small-diameter biodegradable scaffolds for functional vascular tissue engineering in the mouse model, Biomaterials 29 (2008) 1454–1463.
[17] W. Amass, A. Amass, B. Tighe, A review of biodegradable polymers: uses, current developments in the synthesis and characterization of biodegradable polyesters, blends of biodegradables polymers and recent advances in biodegradation studies, Polym. Int. 47 (1998) 89–114.
[18] B. Gupta, N. Revagade, J. Hilborn, Poly(lactic acid) fiber: an overview, Prog. Polym. Sci. 32 (2007) 455–482.
[19] M. Savioli Lopesa, A.L. Jardini, R. Maciel Filho, Poly (lactic acid) production for tissue engineering applications, Procedia Eng. 42 (2012) 1402–1413.
[20] D. Suarez Bagnasco, F. Montini Ballarin, L.J. Cymberknop, G. Balay, C. Negreira, G.A. Abraham, R.L. Armentano, Mechanical properties assessment of electrospun nanofibrous vascular grafts: a comparison with femoral ovine arteries, March 2014. (submitted for publication).
[21] R.J. Zdrahala, I.J. Zdrahala, Biomedical applications of polyurethanes: a review of past promises, present realities, and a vibrant future, J. Biomater. Appl. 14 (1999) 67–90.
[22] S.A. Guelcher, Biodegradable polyurethanes: synthesis and applications in regenerative medicine, Tissue Eng. Part B 14 (2008) 3–17.
[23] J.W. Boretos, W.S. Pierce, Segmented polyurethane: a new elastomer for biomedical applications, Science 158 (1967) 1481–1482.
[24] G.A. Abraham, P.M. Frontini, T.R. Cuadrado, Physical and mechanical behavior of sterilized biomedical segmented polyurethanes, J. Appl. Polym. Sci. 65 (1997) 1193–1203.
[25] P.C. Caracciolo, F. Buffa, G.A. Abraham, Effect of the hard segment chemistry and structure on the thermal and mechanical properties of novel biomedical segmented poly(esterurethanes), J. Mater. Sci. Mater. Med. 20 (2009) 145–155.
[26] D. Annis, A. Bornat, R.O. Edwards, A. Higham, B. Loveday, J. Wilson, An elastomeric vascular prosthesis, Trans. Am. Soc. Artif. Intern. Organs 24 (1978) 209–214.
[27] T.V. How, D. Annis, Viscoelastic behavior of polyurethane vascular prostheses, J. Biomed. Mater. Res. 21 (1987) 1093–1108.
[28] T. Matsuda, M. Ihara, H. Inoguchi, I.K. Kwon, K. Takamizawa, S. Kidoaki, Mechanoactive scaffold design of small-diameter artificial graft made of electrospun segmented polyurethane fabrics, J. Biomed. Mater. Res. 73A (2005) 125–131.
[29] S. Kidoaki, I.K. Kwon, T. Matsuda, Mesoscopic spatial designs of nano-and microfiber meshes for tissue-engineering matrix and scaffold based on newly devised multilayering and mixing electrospinning techniques, Biomaterials 26 (2005) 37–46.
[30] P.C. Caracciolo, V. Thomas, Y.K. Vohra, F. Buffa, G.A. Abraham, Electrospinning of novel biodegradable poly(ester urethane)s and poly(ester urethane urea)s for soft tissue-engineering applications, J. Mater. Sci. Mater. Med. 20 (2009) 2129–2137.
[31] P.C. Caracciolo, F. Buffa, V. Thomas, Y.K. Vohra, G.A. Abraham, Biodegradable polyurethanes: comparative study of electrospun scaffolds and films, J. Appl. Polym. Sci. 121 (2011) 3292–3299.
[32] J.J. Stankus, J. Guan, W.R. Wagner, Fabrication of biodegradable elastomeric scaffolds with sub-micron morphologies, J. Biomed. Mater. Res. 70A (2004) 603–614.
[33] T. Courtney, M.S. Sacks, J.J. Stankus, J. Guan, W.R. Wagner, Design and analysis of tissue engineering scaffolds that mimic soft tissue mechanical anisotropy, Biomaterials 27 (2006) 3631–3638.

[34] M.J. McClure, S.A. Sell, D.G. Simpson, B.H. Walpoth, G.L. Bowlin, A three-layered electrospun matrix to mimic native arterial architecture using polycaprolactone, elastin, and collagen: a preliminary study, Acta Biomater. 6 (2010) 2422–2433.
[35] G.M. Fisher, J.G. Llaurado, Collagen and elastin content in canine arteries selected from functionally different vascular beds, Circ. Res. 19 (1966) 394–399.
[36] J.A.G. Rhodin, Architecture of the vessel wall, Comprehensive Physiology, J. Wiley, New York, 2011, pp. 1–31.
[37] M.J. McClure, D.G. Simpson, G.L. Bowlin, Tri-layered vascular grafts composed of polycaprolactone, elastin, collagen, and silk: optimization of graft properties, J. Mech. Behav. Biomed. Mater. 10 (2012) 48–61.
[38] M.A. Gonzalez, F. Montini Ballarin, M. Brun, G. Abraham, V.L. Ballarin, Morphological quantification of polymer nanofibers in tissue engineering images, Lat. Am. Appl. Res. 42 (2012) 89–95.
[39] H. Wu, J. Fan, C.-C. Chu, Electrospinning of small diameter 3-D nanofibrous tubular scaffolds with controllable nanofiber orientations for vascular grafts, J. Mater. Sci. Mater. Med. 21 (2010) 3207–3215.
[40] E.W. Fischer, H.J. Sterzel, G. Wegner, Kolloid Z. Z. Polym. 251 (1973) 980–990.
[41] D.W. Van Krevelen, K. te Nijenhuis (Eds.), Properties of Polymers, 4th ed., Elsevier, Amsterdam, The Netherlands, 2009, p. 121.
[42] X. Zong, K. Kim, D. Fang, S. Ran, B.S. Hsiao, B. Chu, Structure and process relationship of electrospun bioabsorbable nanofiber membranes, Polymer 43 (2002) 4403–4412.
[43] H. Zhuo, J. Hu, S. Chen, Electrospun polyurethane nanofibres having shape memory effect, Mater. Lett. 62 (2008) 2074–2076.
[44] L. Liu, Y. Ren, Y. Li, Y. Liang, Effects of hard and soft components on the structure formation, crystallization behavior and mechanical properties of electrospun poly(L-lactic acid) nanofibers, Polymer 54 (2013) 5250–5256.
[45] M. Shibata, N. Teramoto, Y. Inoue, Mechanical properties, morphologies, and crystallization behavior of plasticized poly(L-lactide)/poly(butylene succinate-co-L-lactate) blends, Polymer 48 (2007) 2768–2777.
[46] C.-C. Chen, J.-Y. Chueh, H. Tseng, H.-M. Huang, S.-Y. Lee, Preparation and characterization of biodegradable PLA polymeric blends, Biomaterials 24 (2003) 1167–1173.

Florencia Montini Ballarin: Florencia received her bachelor degree in 2009 at the School of Engineering, National University of Mar del Plata, Argentina, and now is a postgraduate student, at the Research Institute for Materials Science and Technology (INTEMA). Her main research interests are on electrospinning processing technique, polymeric and composite biomaterials, tissue engineering and mechanical, physical and thermal characterization of biomaterials at present.

Pablo C. Caracciolo: Pablo received his PhD degree in Materials Science at the Materials Department of the School of Engineering, National University of Mar del Plata, Argentina and his bachelor degree at the School of Exact and Natural Sciences, National University of Mar del Plata. He is now an assistant researcher for the National Research Council (CONICET) at the Research Institute for Materials Science and Technology (INTEMA). His main research interests are on polymeric and composite nanofibers for tissue engineering and functional textile applications and bioresorbable biomedical polyurethanes, non-viral gene delivery, and biocompatible drug delivery systems.

Eduardo Blotta: Eduardo received his PhD degree in Engineering and his bachelor's degree at the Electronics Department of the School of Engineering, National University of Mar del Plata, Argentina. He is working at the Digital Image Processing Group of the Electronics Department. He is an Associate Professor of the Electronics Department. His research interests include Pattern Recognition, Computer Vision, Mathematical Morphology and Speckle Interpherometry.

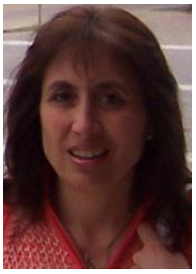

Virginia L. Ballarin: Virginia received his PhD degree in Biological Science at the Biomedical Engineering Department of the National University of Tucuman and his Electronics Engineering degree and Master degree at the National University of Mar del Plata, Argentina. She is a Professor of Scholastic Processes and Digital Image Processing at the Electronics Department of UNMdP. She leads the Digital Image Processing Group at the Electronics Department of UNMdP with research emphasis in mathematical morphology, pattern recognition and medical image processing. She is the President of the Argentinean Society of Bioengineering and also a member of the IEEE Engineering in Medicine and Biology Society.

Gustavo A. Abraham: Gustavo received his PhD degree in Materials Science at the Materials Department of the School of Engineering, National University of Mar del Plata, Argentina and his bachelor's degree at the School of Exact and Natural Sciences, National University of Mar del Plata. He is working at the Research Institute for Materials Science and Technology (INTEMA) as independent researcher for the National Research Council (CONICET). He is an Associate Professor of Chemistry and Biomaterials at the School of Engineering, National University of Mar del Plata, Argentina. His research interests include polymeric biomaterials, scaffolding, tissue engineering, and biomimetic nanomaterials.